

© 2023 Optica Publishing Group. One print or electronic copy may be made for personal use only. Systematic reproduction and distribution, duplication of any material in this paper for a fee or for commercial purposes, or modifications of the content of this paper are prohibited.

Loïc Bodiou, Marion Baillieul, Virginie Nazabal, Jonathan Lemaitre, Albane Benardais, Sofiane Meziani, Nathalie Lorrain, Yannick Dumeige, Petr Nemeč, and Joël Charrier, "Carbon dioxide mid-infrared sensing based on Dy³⁺-doped chalcogenide waveguide photoluminescence," *Opt. Lett.* 48, 1128-1131 (2023), <https://doi.org/10.1364/OL.483613>

Carbon dioxide mid-infrared sensing based on Dy³⁺-doped chalcogenide waveguides photoluminescence

Loïc BODIOU,^{1,*} MARION BAILLIEUL², VIRGINIE NAZABAL,^{3,2,*} JONATHAN LEMAITRE,¹ ALBANE BENARDAIS,³ SOFIANE MEZIANI,¹ NATHALIE LORRAIN,¹ YANNICK DUMEIGE,¹ PETR NEMEC,² AND JOËL CHARRIER¹

¹Univ Rennes, CNRS, Institut FOTON - UMR 6082, F-22305 Lannion, France

²Department of Graphic Arts and Photophysics, Faculty of Chemical Technology, University of Pardubice, 53210 Pardubice, Czech Republic

³Univ Rennes, CNRS, ISCR (Institut des Sciences Chimiques de Rennes) - UMR 6226, F-35000 Rennes, France

*Corresponding authors: loic.bodiou@univ-rennes1.fr; virginie.nazabal@univ-rennes1.fr

Received XX Month XXXX; revised XX Month, XXXX; accepted XX Month XXXX; posted XX Month XXXX (Doc. ID XXXXX); published XX Month XXXX

Climate active gases, notably carbon dioxide (CO₂), methane (CH₄) and nitrous oxide (N₂O), display fundamental absorption bands in the mid-infrared (mid-IR). The detection and monitoring of those gases could be enabled by the development of mid-IR optical sources. Broadband mid-IR on-chip light emission from rare earth-doped chalcogenides photonic integrated circuits could provide a compact, efficient and cost effective gas sensing solution. Mid-IR photoluminescence of dysprosium-doped selenide ridge waveguides obtained under optical pumping at telecommunication wavelength (~1.3 μm) is investigated for Dy³⁺ ion concentrations in the 2500-10000 ppmw range. CO₂ detection around 4.3 μm is then demonstrated based on absorption in this broadband mid-IR emission. © 2022 Optica Publishing Group

<http://dx.doi.org/10.1364/OL.99.099999>

Optical gas sensing systems are receiving increasing attention from both academic and industrial actors because these devices would benefit to widespread application fields ranging from industrial process control to air quality monitoring through greenhouse farming. Economic and environmental concerns require dedicated CH₄ and CO₂ sensors to be deployed for real-time monitoring of costly leaks of natural gas pipelines or aircraft emissions monitoring. To enable compact sensing systems, integrated photonics is a promising solution [1]. Leveraging from the availability of high-quality wafer scale silicon thin films, mature patterning capabilities thanks to fabrication advances of the complementary metal-oxide-semiconductor technology and its potential to monolithically integrate electronics and photonics, silicon platform has emerged as the powerful solution to develop integrated gas sensors in the near-infrared (near-IR) notably for on-chip CH₄ detection around a wavelength of 1.65 μm [2-4]. However, to improve sensor sensitivity and selectivity, CO₂ or CH₄ mid-infrared (mid-IR) fundamental absorptions use, respectively around 4.3 and 3.3 μm, is preferable as their cross-section is orders

of magnitude larger than near-IR overtone vibrations. Si waveguide cross-section tailoring and Si suspended membranes fabrication were thus proposed to provide efficient mid-IR gas sensing [5, 6].

Amorphous chalcogenides (ChG) are commonly selected for a myriad of photonic devices and applications [7]. One of their most interesting optical property, along with their high optical nonlinearity, relies on their wide mid-IR transparency which makes them an alternative and ideal solution for mid-IR sensing of climate active gases [8-12]. However, to implement compact sensing devices, replacement of fibers by integrated waveguides and external (off-chip) lasers by mid-IR on-chip light sources is required. To develop these on-chip mid-IR sources, in particular in the 3-5 μm wavelength range, where fundamental absorption bands of several climate active gases are found, different routes have emerged including supercontinuum generation [13] or interband and quantum cascade lasers [14-15]. Using different rare earth ions, notably Tm³⁺, Ho³⁺, Nd³⁺, Er³⁺, Dy³⁺ or Pr³⁺, broadband mid-IR emission has also been demonstrated in different materials ranging from oxides to fluorides [16]. Thanks to their lower phonon energy, amorphous ChG further favor long-wavelength radiative transitions from rare earth ions [17]. In particular, lasing up to ~5.4 μm and emissions up to 8 μm were recently demonstrated in ChG fibers notably based on Tb³⁺, Ce³⁺, Dy³⁺ or Sm³⁺ transitions [18-20].

Development of photonic integrated circuits made of mid-IR emitting rare earth-doped ChG may therefore be a key enabler in the implementation of climate active gases monitoring devices with reduced size, weight, power consumption and cost [21]. Praseodymium-doped selenides integrated ridge waveguides have been demonstrated to display broadband mid-IR emission in the 2-5.5 μm wavelength range [22, 23]. Mid-IR luminescence was also reported from Dy³⁺ ions in ChG bulk materials and fibers [18, 24-26] but, to our knowledge, no demonstration of mid-IR Dy³⁺ emission from integrated ChG waveguides has been published yet.

In this Letter, fabrication of integrated ridge waveguides based on RF magnetron sputtered Dy³⁺-doped Ga₅Ge₂₀Sb₁₀Se₆₅ amorphous thin films is presented. Dy³⁺ mid-IR luminescence in the 2.2-3 μm and 4-4.8 μm wavelength ranges obtained from integrated

ridge waveguides is subsequently investigated with regards to Dy³⁺ ion doping concentrations. Finally, Dy³⁺ broadband mid-IR emission around 4.3 μm is used to demonstrate CO₂ sensing capability of these devices for CO₂ concentrations up to 0.4 %.

The melt and quenching technique was used to prepare two bulk glasses from the Ga-Ge-Sb-Se quaternary system with a targeted nominal glass composition of Ga₅Ge₂₀Sb₁₀Se₆₅. Dysprosium was used to dope one of the bulks with a concentration of 10000 ppmw (parts per million by weight). Sputtering targets of 50-mm diameter were obtained after polishing slices of the bulks. RF magnetron co-sputtering was then performed, at room temperature under 5×10⁻³ mbar Ar pressure, on thermally oxidized (2-μm thick SiO₂) 2" silicon wafer using a three-cathode co-sputtering cluster exploiting two undoped targets and one 10000 ppmw Dy³⁺-doped Ga₅Ge₂₀Sb₁₀Se₆₅ target. Different Dy³⁺ ion doping concentrations in the 2500-10000 ppmw range in the sputtered thin film were obtained by simultaneously applying different powers on the three cathodes (Table 1). Composition of co-sputtered thin films which was determined via energy-dispersive X-Ray analysis showed a good agreement with the glass targets (Table 1).

Table 1. Summary of RF magnetron co-sputtering conditions used for GaGeSbSe:Dy³⁺ thin films deposition

Dy ³⁺ estimated concentration (ppmw)	Applied power (W) on cathode			Thin film composition (at%) ±1%	Thickness (nm) ±10 nm
	#1 Dy ³⁺ doped	#2 undoped	#3 undoped		
2500	10	12	12	Ga ₅ Ge ₁₉ Sb ₆ Se ₇₀	1145
5000	15	10	8	Ga ₆ Ge ₂₀ Sb ₆ Se ₆₈	1150
7500	15	8	0	Ga ₆ Ge ₂₁ Sb ₆ Se ₆₇	1110
10000	15	0	0	Ga ₇ Ge ₂₁ Sb ₅ Se ₆₇	1530

To select the optimal excitation wavelength to be used during photoluminescence (PL) experiments, the absorption spectrum of a Dy³⁺-doped Ga₅Ge₂₀Sb₁₀Se₆₅ (10000 ppmw) glass target was recorded using UV/Visible/near-IR spectrophotometer (Fig. 1).

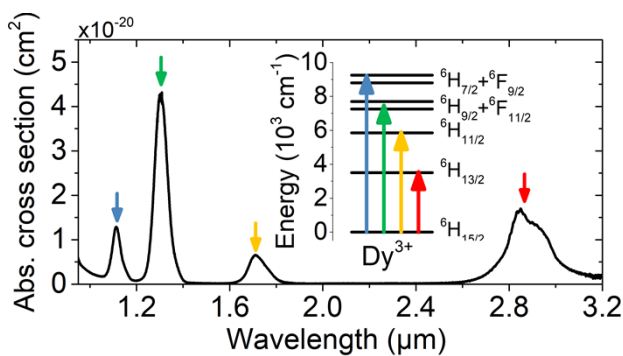


Fig. 1. Absorption spectrum of the Ga₅Ge₂₀Sb₁₀Se₆₅:Dy³⁺ glass target (10000 ppmw ion doping concentration). Inset: simplified low energy part of the energy level diagram of Dy³⁺ ions.

This absorption spectrum displays the characteristic absorption bands of the 4f electron configuration of Dy³⁺ ions [27]. In particular, strong absorption is observed around 1.3 μm (represented as a green arrow in Fig. 1) corresponding to the transition from the ground state (⁶H_{15/2}) to the thermally coupled ⁶H_{9/2} and ⁶F_{11/2} energy levels. This transition is particularly convenient as it corresponds to

a wavelength at which many lasers, notably integrated on Si [28], have been developed for datacom applications. Transitions from the ground state ⁶H_{15/2} to the thermally coupled ⁶H_{7/2}+⁶F_{9/2}, ⁶H_{11/2} and ⁶H_{13/2} manifolds can be seen around 1.1, 1.7 and 2.85 μm (respectively represented in blue, yellow and red arrows in Fig. 1).

Ridge waveguides of different widths (w) were subsequently fabricated, following the procedure described in [22], using standard i-line photolithographic process and dry etching (Fig. 2a).

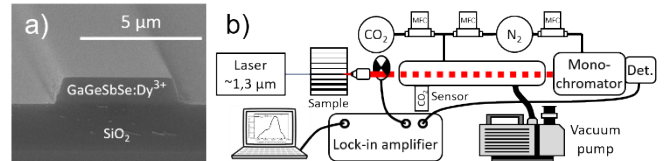


Fig. 2. a) Scanning electron microscope picture of a Dy³⁺-doped GaGeSbSe ridge waveguide. b) Optical set-up enabling CO₂ concentration-dependent PL measurements,

Photoluminescence (PL) experiments were performed on 5-mm long samples using a tunable pump laser emitting an optical power of 20 mW around 1.3 μm. All presented PL spectra were recorded at room temperature as no spectral nor intensity significant evolution was observed in the studied temperature range (10-60°C). Light generated on-chip was collected by an aspheric lens and detected by an InSb photodiode after passing through a 65-cm long tube-shaped vacuum chamber that can be pumped and/or filled with various gaseous dilutions of CO₂ in N₂ and a spectrometer equipped with several long-pass filters to avoid the recording of unwanted harmonic contributions. To improve signal to noise ratio, lock-in technique was used (Fig. 2b).

Photoluminescence spectra were first recorded between 2.1 and 3.2 μm for multiple excitation wavelengths separated by 5 nm and tuned around 1.3 μm. The resulting photoluminescence excitation (PLE) spectroscopy map is displayed in Fig. 3a).

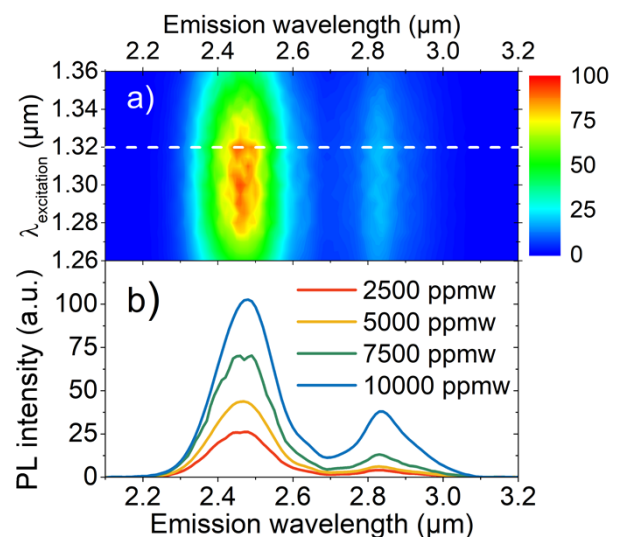


Fig. 3. a) PL excitation spectroscopy map recorded in the 2.1-3.2 μm wavelength range ([Dy³⁺]=7500 ppmw), b) PL spectra (λ_{exc}=1320 nm) for 8-μm wide ridge waveguides with four Dy³⁺ ion concentrations.

Fig. 3a) was obtained for a 9- μm wide ridge waveguide and Dy^{3+} ion concentration of 7500 ppmw. However, this result is representative of PLE maps recorded for others Dy^{3+} doping levels and waveguide widths. Fig. 3a) confirms the possibility to generate mid-IR emission from Dy^{3+} ions in GaGeSbSe amorphous matrix by using a pumping wavelength around 1.3 μm and that excitation wavelengths between 1280 and 1320 nm lead to the maximum PL signal. From Fig. 3a), one can further observe two broad PL bands centered at 2.46 and 2.84 μm , corresponding, respectively, to the ${}^6\text{F}_{11/2}+{}^6\text{H}_{9/2}\rightarrow{}^6\text{H}_{13/2}$ and ${}^6\text{H}_{13/2}\rightarrow{}^6\text{H}_{15/2}$ transitions. Fig. 3b) displays the PL spectra recorded from 8- μm wide waveguides for the 4 samples with Dy^{3+} ions concentrations ranging from 2500 to 10000 ppmw using an excitation wavelength of 1320 nm, represented by the white dashed line in Fig. 3a). An almost linear increase of PL intensity with Dy^{3+} concentration can be inferred from Fig. 3b). As ridge waveguide of different widths were patterned on each sample, this experiment was reproduced for several waveguides of widths larger than 5 μm , i.e. operating in the multimode region at both pump and signal wavelengths [22], and gave a similar trend of PL enhancement with Dy^{3+} doping level. It should be noted that investigation of larger doping concentrations was limited by the concentration introduced in the bulk during the synthesis.

Fig. 4 displays PL spectra recorded, with the tube-shaped chamber filled with ambient laboratory air, for wavelengths above 3.8 μm . The PL observed in this spectral domain corresponds to the transition between the ${}^6\text{H}_{11/2}$ and ${}^6\text{H}_{13/2}$ manifolds. As previously observed in the 2.2-3.1 μm wavelength range, an increase of the PL intensity with Dy^{3+} content in GaGeSbSe waveguides is found in this spectral domain without any obvious saturation effect suggesting that higher Dy^{3+} concentrations might be beneficial to further increase mid-IR emission.

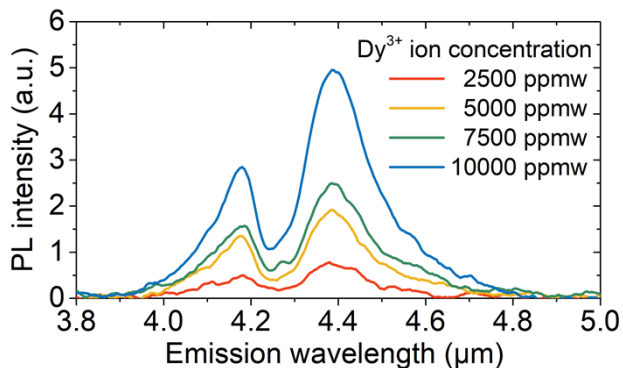


Fig. 4. Mid-IR PL spectra ($\lambda_{\text{exc}}=1320$ nm) for 8- μm wide ridge waveguides with four Dy^{3+} ion concentrations.

The same experiment was reproduced with waveguides of varying width. Interestingly, PL emission was observed, for all Dy^{3+} concentrations, for waveguide widths down to 1.5-2 μm that only support singlemode propagation above 4 μm [22]. Emission above 5 μm , originating from the ${}^6\text{F}_{11/2}+{}^6\text{H}_{9/2}\rightarrow{}^6\text{H}_{11/2}$ transition [18], was not clearly observed during the experiments probably due to reduced InSb detector sensitivity in this wavelength range. It is well established that the absorption attributed to Se-H bonds vibrations is located at 4.5 μm [29] and this negatively affects emission broadening towards long wavelengths and PL signal collection around 4.5 μm . A dip in the PL spectra

overlapping CO_2 absorption around 4.3 μm [30] can be observed in all PL spectra resulting from the presence of CO_2 at ambient atmospheric level concentration (~ 410 ppm) in the mid-IR beam path during the experiments. Due to the waveguide length and low evanescent power factor [1], below $\sim 10\%$ for all waveguides dimensions and around 5% for $w=8$ μm , evanescent sensing only slightly accounts for the observed absorption. This emphasizes that Dy^{3+} PL could be used to enable CO_2 sensing based on absorption spectroscopy as previously demonstrated using ChG fibers [9, 10].

To avoid undesirable absorption of Dy^{3+} mid-IR emission by CO_2 molecules along free-space propagation between ridge waveguide output facet and detector (through spectrometer), N_2 flow was used to purge the spectrometer during following experiments. Furthermore, using a rotary pump, a primary vacuum of about 10 Pa was produced in the tube-shaped vacuum chamber. To monitor CO_2 concentration along the free-space propagation, a Sensiron SCD30 was placed inside the tube (Fig. 2b). During PL measurements, vacuum pump was stopped to prevent vibrations that hinder efficient light injection in waveguides. The tube was progressively filled with a gaseous mixture of N_2 and CO_2 using mass flow controllers. Emission spectra from recorded, in the 3.8-5.0 μm wavelength range, for different CO_2 concentrations in the beam path, i.e. in the tube, are presented in Fig. 5.

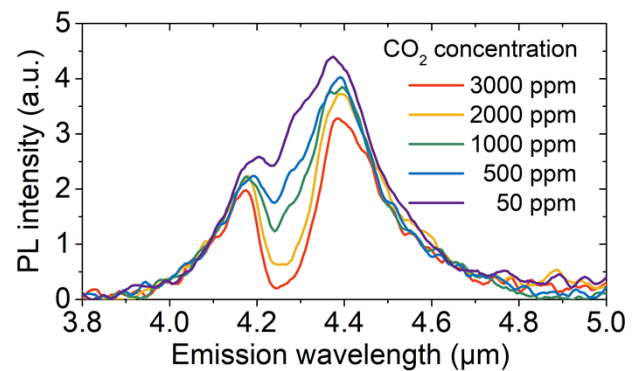


Fig. 5. Mid-IR PL spectra ($\lambda_{\text{exc}}=1320$ nm) for different CO_2 concentrations for a 7- μm wide waveguide ($[\text{Dy}^{3+}]=10000$ ppmw).

As CO_2 concentration increases, a clear reduction of PL signal is observed around 4.3 μm , which overlaps the spectral range where light absorption by CO_2 molecules is maximal [6, 18, 30]. This spectral evolution confirms that vibrational absorption of CO_2 molecules found along the free-space propagation between waveguide output facet and spectrometer entrance was responsible for the dip observed on mid-IR Dy^{3+} emission spectra in Fig. 4. It can also be noticed that PL spectra were recorded for a minimal CO_2 concentration of 50 ppm, corresponding to the residual CO_2 concentration found during the experiments due to incomplete purging of the set-up. From Fig. 5, it is clearly observed that Dy^{3+} PL remains unaffected by CO_2 build-up for wavelengths below 4.15 μm and above 4.45 μm . To emphasize this effect, monitoring of Dy^{3+} PL intensity with CO_2 content in the beam path was performed at 4.25 and 4.45 μm (Fig. 6).

The Dy^{3+} PL intensity recorded at a wavelength corresponding to maximum CO_2 absorption (4.25 μm) follows a logarithmic evolution conforming to Beer-Lambert law whereas, at 4.45 μm , light emission from Dy^{3+} ions is found to be independent of CO_2

concentration encountered along the beam path. Implementation of Dy³⁺-doped GaGeSbSe waveguide-based multimode interferometers (MMI) to multiplex mid-IR light [21] could enable calibration-free CO₂ sensing by simultaneously monitoring Dy³⁺ mid-IR emission at $\lambda \sim 4.25 \mu\text{m}$ and $\lambda \sim 4.45 \mu\text{m}$ corresponding, respectively, to spectral bands overlapping and not affected by CO₂ absorption. Pr³⁺-doped ChG waveguides were demonstrated [22, 10] to provide PL emission around absorption maxima of CO (4.6 μm) and CH₄ (3.3 μm), Pr³⁺ co-doping could therefore enhance device versatility by allowing multigas sensing.

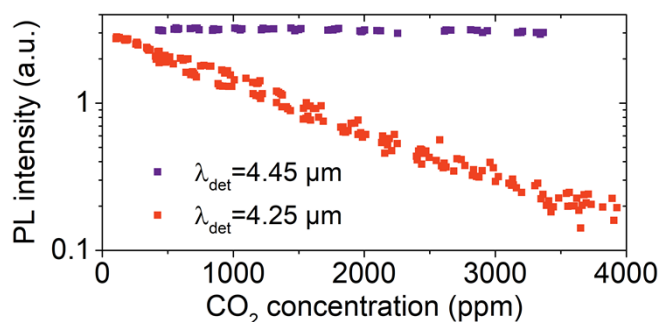


Fig. 6. Mid-IR PL detected at 4.25 and 4.45 μm ($\lambda_{\text{exc}}=1320 \text{ nm}$) for a 7- μm wide ridge waveguide for different CO₂ concentrations.

In conclusion, Dy³⁺-doped Ga₅Ge₂₀Sb₁₀Se₆₅ ridge waveguides with Dy³⁺ concentration ranging from 2500 to 10000 ppmw have been fabricated. These waveguides enabled the recording of mid-IR emission between 3.8 to 5.0 μm under near-IR pumping around 1.3 μm in waveguides exhibiting singlemode propagation at $\sim 4.4 \mu\text{m}$. An almost linear increase of mid-IR luminescence with Dy³⁺ concentration was found for multimode waveguides. Based on this on-chip emission, CO₂ mid-IR sensing demonstration was performed confirming the potential of Dy³⁺-doped ChG waveguides for the development of compact optical gas sensors.

Funding. Financial support was received from CNRS through the MITI interdisciplinary programs (ORIGAMI), French national research agency under MID-VOC and KASHMIR ANR projects (ANR-17-CE09-0028-01 and ANR-22-CE24-0021) and Czech Science Foundation (project No. 22-05179S).

Acknowledgments. This work was partly supported by the French Renatech+ network. S.M. acknowledges financial support from Lannion Trégor Communauté and Région Bretagne (grant DESIR).

Disclosures. The authors declare no conflicts of interest

References

1. V. Passaro, C. Tullio, B. Troia, M. Notte, G. Giannoccaro, and F. Leonardi, *Sensors* **12**, 15558 (2012). [doi](#)
2. L. Tombez, E. J. Zhang, J. S. Orcutt, S. Kamlapurkar, and W. M. J. Green, *Optica* **4**, 1322 (2017). [doi](#)
3. E.J. Zhang, Y. Martin, J.S Orcutt, C. Xiong, M. Glodde, T. Barwicz, L. Schares, E.A. Duch, N. Marchack, C.C Teng, Proceedings of the Conference on Lasers and Electro-Optics, OSA, San Jose, CA, USA, 5–10 May 2019; p. ST1F.2. [doi](#)
4. W.-C. Lai, S. Chakravarty, X. Wang, C. Lin, and Ray T. Chen, *Opt. Lett.* **36**,

- 984 (2011) [doi](#)
5. T. Jin, J. Zhou and P. T. Lin, *RSC Adv.* **10**, 7452 (2020). [doi](#)
6. F. Ottonello-Briano, C. Errando-Herranz, H. Rödjegård, H. Martin, H. Sohlström, and K. B. Gylfason, *Opt. Lett.* **45**, 109 (2020). [doi](#)
7. B. Eggleton, B. Luther-Davies, K. Richardson, *Nat Photon* **5**, 141 (2011). [doi](#)
8. L. Wang, W. Ma, P. Zhang, L. Zhu, D. Yang, X. Wang, S. Dai, *Journal Lightwave Technol.* **37**, 5193, (2019). [doi](#)
9. F. Starecki, F. Charpentier, J.-L. Doualan, L. Quétel, K. Michel, R. Chahal, J. Troles, B. Bureau, A. Braud, P. Camy, V. Moizan, V. Nazabal, *Sensors and Actuators B: Chemical* **207**, 518 (2015). [doi](#)
10. J. Ari, F. Starecki, C. Boussard-Plédel, Y. Ledemi, Y. Messaddeq, J.-L. Doualan, A. Braud, B. Bureau, V. Nazabal, *Opt. Lett.* **43**, 2893 (2018) [doi](#)
11. Z. Han, P. Lin, V. Singh, L. Kimerling, J. Hu, K. Richardson, A. Agarwal, and D. T. H. Tan, *Appl. Phys. Lett.* **108**, 141106 (2016). [doi](#)
12. P. Su, Z. Han, D. Kita, P. Becla, H. Lin, S. Deckoff-Jones, K. Richardson, L. C. Kimerling, J. Hu, A. Agarwal, *Appl. Phys. Lett.* **114**, 051103 (2019). [doi](#)
13. C. Lafforgue, M. Montesinos-Ballester, T.-T.-D. Dinh, X. Le Roux, E. Cassan, D. Marris-Morini, C. Alonso-Ramos, and L. Vivien, *Photon. Res.* **10**, A43 (2022). [doi](#)
14. A. Spott, E. J. Stanton, A. Torres, M. L. Davenport, C. L. Canedy, I. Vurgafman, M. Kim, C. S. Kim, C. D. Merritt, W. W. Bewley, J. R. Meyer, and J. E. Bowers, *Optica* **5**, 996 (2018) [doi](#)
15. A. Spott, Jon Peters, M. L. Davenport, E. J. Stanton, C. D. Merritt, W. W. Bewley, I. Vurgafman, C. S. Kim, J. R. Meyer, J. Kirch, L. J. Mawst, D. Botez, and J. E. Bowers, *Optica* **3**, 545 (2016). [doi](#)
16. S. Jackson, *Nature Photon.* **6**, 423 (2012). [doi](#)
17. V. Nazabal and J.-L. Adam, *Optical Materials: X* **15**, 100168 (2022). [doi](#)
18. F. Starecki, G. Louvet, J. Ari, A. Braud, J.-L. Doualan, R. Chahal, I. Hafienne, C. Boussard, V. Nazabal, P. Camy, *J. Lumin.*, **218**, 116853 (2020). [doi](#)
19. V.S. Shiryayev, M.V. Sukhanov, A.P. Velmuzhov, E.V. Karakina, T.V. Kotereva, G.E. Snopatin, B.I. Denker, B.I. Galagan, S.E. Sverchkov, V.V. Koltashev, V.G. Plotnichenko, *J. Non-Cryst. Solids* **567**, 120939 (2021). [doi](#)
20. J.J. Nunes, Ł. Sojka, R.W. Crane, D. Furniss, Z.Q. Tang, D. Mabwa, B. Xiao, T. M. Benson, M. Farries, N. Kalfagiannis, E. Barney, S. Phang, A.B. Seddon, S. Sujecki, *Opt. Lett.* **46**, 3504 (2021). [doi](#)
21. L. Bodiou, Y. Dumeige, S. Normani, G. Louvet, P. Němec, V. Nazabal, and J. Charrier, *IEEE Sensors Journal* **20**, 13426 (2020) [doi](#)
22. L. Bodiou, F. Starecki, J. Lemaître, V. Nazabal, J.-L. Doualan, E. Baudet, R. Chahal, A. Gutierrez-Arroyo, Y. Dumeige, I. Hardy, A. Braud, R. Soulard, P. Camy, P. Němec, G. Palma, F. Prudenzano, J. Charrier, *Optical Materials* **75**, 109 (2018). [doi](#)
23. G. Louvet, S. Normani, L. Bodiou, J. Gutwirth, J. Lemaître, P. Pirasteh, J.-L. Doualan, A. Benardais, Y. Ledemi, Y. Messaddeq, P. Němec, J. Charrier, and V. Nazabal, *Opt. Express* **28**, 22511 (2020). [doi](#)
24. L. Sojka, Z. Tang, D. Jayasuriya, M. Shen, D. Furniss, E. Barney, T.M. Benson, A.B. Seddon, S. Sujecki, *Opt. Mater. Express* **9**, 2291 (2019). [doi](#)
25. H. Guo, L. Liu, Y. Wang, C. Hou, W. Li, M. Lu, K. Zou, and B. Peng, *Opt. Express* **17**, 15350 (2009). [doi](#)
26. M. Sun, A. Yang, H. Ren, Sisheng Qi, H. Lin, X. Feng, Zhiyong Yang, *Journal of Non-Crystalline Solids* **560**, 120718 (2021) [doi](#)
27. T. Schweizer, D. W. Hewak, B. N. Samson, and D. N. Payne, *Opt. Lett.* **21**, 1594 (1996). [doi](#)
28. Y. Wan, J.C. Norman, Y. Tong, M.J. Kennedy, W. He, J. Selvidge, C. Shang, M. Dumont, A. Malik, H.K. Tsang, A.C. Gossard, J.E. Bowers, *Laser & Photonics Reviews* **14**, 2000037 (2020). [doi](#)
29. B. Cole, L.B. Shaw, P.C. Pureza, R. Mossadegh, J.S. Sanghera, I.D. Aggarwal, *Journal of Non-Crystalline Solids* **256**, 253 (1999). [doi](#)
30. R.V. Kochanov, I.E. Gordon, L.S. Rothman, P. Wcislo, C. Hill, J.S. Wilzewski, *J. Quant. Spectrosc. Radiat. Transfer* **177**, 15-30 (2016) [doi](#)

1. V. Passaro, C. Tullio, B. Troia, M. Notte, G. Giannoccaro, and F. Leonardis, "Recent Advances in Integrated Photonic Sensors," *Sensors* **12**, 15558–15598 (2012). [doi](#)
2. L. Tombez, E. J. Zhang, J. S. Orcutt, S. Kamapurkar, and W. M. J. Green, "Methane absorption spectroscopy on a silicon photonic chip," *Optica* **4**, 1322 (2017). [doi](#)
3. E.J. Zhang, Y. Martin, J.S Orcutt, C. Xiong, M. Glodde, T. Barwicz, L. Schares, E.A. Duch, N. Marchack, C.C Teng, "Trace-Gas Spectroscopy of Methane Using a Monolithically Integrated Silicon Photonic Chip Sensor," Proceedings of the Conference on Lasers and Electro-Optics, OSA, San Jose, CA, USA, 5–10 May 2019; p. STh1F.2. [doi](#)
4. W.-C. Lai, S. Chakravarty, X. Wang, C. Lin, and Ray T. Chen, "On-chip methane sensing by near-IR absorption signatures in a photonic crystal slot waveguide," *Opt. Lett.* **36**, 984 (2011) [doi](#)
5. T. Jin, J. Zhou and P. T. Lin, "Real-time and non-destructive hydrocarbon gas sensing using mid-infrared integrated photonic circuits," *RSC Adv.* **10**, 7452 (2020). [doi](#)
6. F. Ottonello-Briano, C. Errando-Herranz, H. Rödjegård, H. Martin, H. Sohlström, and K. B. Gylfason, "Carbon dioxide absorption spectroscopy with a mid-infrared silicon photonic waveguide," *Opt. Lett.* **45**, 109 (2020). [doi](#)
7. B. Eggleton, B. Luther-Davies, K. Richardson, "Chalcogenide photonics," *Nat Photon* **5**, 141 (2011). [doi](#)
8. L. Wang, W. Ma, P. Zhang, L. Zhu, D. Yang, X. Wang, S. Dai, "Mid-Infrared Gas Detection Using a Chalcogenide Suspended-Core Fiber," *Journal Lightwave Technol.* **37**, 5193, (2019). [doi](#)
9. F. Starecki, F. Charpentier, J.-L. Doualan, L. Quétel, K. Michel, R. Chahal, J. Troles, B. Bureau, A. Braud, P. Camy, V. Moizan, V. Nazabal, "Mid-IR optical sensor for CO₂ detection based on fluorescence absorbance of Dy³⁺:Ga₅Ge₂₀Sb₁₀S₆₅ fibers," *Sensors and Actuators B: Chemical* **207**, 518 (2015). [doi](#)
10. J. Ari, F. Starecki, C. Boussard-Plédel, Y. Ledemi, Y. Messaddeq, J.-L. Doualan, A. Braud, B. Bureau, and V. Nazabal, "Co-doped Dy³⁺ and Pr³⁺ Ga₅Ge₂₀Sb₁₀S₆₅ fibers for mid-infrared broad emission," *Opt. Lett.* **43**, 2893-2896 (2018) [doi](#)
11. Z. Han, P. Lin, V. Singh, L. Kimerling, J. Hu, K. Richardson, A. Agarwal, and D. T. H. Tan, "On-chip mid-infrared gas detection using chalcogenide glass waveguide," *Appl. Phys. Lett.* **108**, 141106 (2016). [doi](#)
12. P. Su, Z. Han, D. Kita, P. Becla, H. Lin, S. Deckoff-Jones, K. Richardson, L. C. Kimerling, J. Hu, A. Agarwal, "Monolithic on-chip mid-IR methane gas sensor with waveguide-integrated detector," *Appl. Phys. Lett.* **114**, 051103 (2019). [doi](#)
13. C. Laffogues, M. Montesinos-Ballester, T.-T.-D. Dinh, X. Le Roux, E. Cassan, D. Marris-Morini, C. Alonso-Ramos, and L. Vivien, "Supercontinuum generation in silicon photonics platforms," *Photon. Res.* **10**, A43 (2022). [doi](#)
14. A. Spott, E. J. Stanton, A. Torres, M. L. Davenport, C. L. Canedy, I. Vurgaftman, M. Kim, C. S. Kim, C. D. Merritt, W. W. Bewley, J. R. Meyer, and J. E. Bowers, "Interband cascade laser on silicon," *Optica* **5**, 996 (2018) [doi](#)
15. A. Spott, Jon Peters, M. L. Davenport, E. J. Stanton, C. D. Merritt, W. W. Bewley, I. Vurgaftman, C. S. Kim, J. R. Meyer, J. Kirch, L. J. Mawst, D. Botez, and J. E. Bowers, "Quantum cascade laser on silicon," *Optica* **3**, 545 (2016). [doi](#)
16. S. Jackson, "Towards high-power mid-infrared emission from a fibre laser," *Nature Photon.* **6**, 423 (2012). [doi](#)
17. V. Nazabal and J.-L. Adam, "Infrared luminescence of chalcogenide glasses doped with rare earth ions and their potential applications," *Optical Materials: X* **15**, 100168 (2022). [doi](#)
18. F. Starecki, G. Louvet, J. Ari, A. Braud, J.-L. Doualan, R. Chahal, I. Hafienne, C. Boussard, V. Nazabal, P. Camy, "Dy³⁺ doped GaGeSbSe fiber long-wave infrared emission," *J. Lumin.*, **218**, 116853 (2020). [doi](#)
19. V.S. Shiryayev, M.V. Sukhanov, A.P. Velmuzhov, E.V. Karaksina, T.V. Kotereva, G.E. Snopatin, B.I. Denker, B.I. Galagan, S.E. Sverchkov, V.V. Koltashev, V.G. Plotnichenko, "Core-clad terbium doped chalcogenide glass fiber with laser action at 5.38 μm," *J. Non-Cryst. Solids* **567**, 120939 (2021). [doi](#)
20. J.J. Nunes, Ł. Sojka, R.W. Crane, D. Furniss, Z.Q. Tang, D. Mabwa, B. Xiao, T. M. Benson, M. Farries, N. Kalfagiannis, E. Barney, S. Phang, A.B. Seddon, S. Sujecki, "Room temperature mid-infrared fiber lasing beyond 5 μm in chalcogenide glass small-core step index fiber," *Opt. Lett.* **46**, 3504 (2021). [doi](#)
21. L. Bodiou, Y. Dumeige, S. Normani, G. Louvet, P. Němec, V. Nazabal, and J. Charrier, "Design of a Multimode Interferometer-Based Mid-Infrared Multispecies Gas Sensor," *IEEE Sensors Journal* **20**, 13426 (2020) [doi](#)
22. L. Bodiou, F. Starecki, J. Lemaître, V. Nazabal, J.-L. Doualan, E. Baudet, R. Chahal, A. Gutierrez-Arroyo, Y. Dumeige, I. Hardy, A. Braud, R. Souillard, P. Camy, P. Němec, G. Palma, F. Prudenzano, J. Charrier, "Mid-infrared guided photoluminescence from integrated Pr³⁺-doped selenide ridge waveguides," *Optical Materials* **75**, 109 (2018). [doi](#)
23. G. Louvet, S. Normani, L. Bodiou, J. Gutwirth, J. Lemaître, P. Pirasteh, J.-L. Doualan, A. Benardais, Y. Ledemi, Y. Messaddeq, P. Němec, J. Charrier, and V. Nazabal, "Co-sputtered Pr³⁺-doped Ga-Ge-Sb-Se active waveguides for mid-infrared operation," *Opt. Express* **28**, 22511 (2020). [doi](#)
24. L. Sojka, Z. Tang, D. Jayasuriya, M. Shen, D. Furniss, E. Barney, T.M. Benson, A.B. Seddon, S. Sujecki, "Ultra-broadband mid-infrared emission from a Pr³⁺/Dy³⁺ co-doped selenide-chalcogenide glass fiber spectrally shaped by varying the pumping arrangement [Invited]," *Opt. Mater. Express* **9**, 2291 (2019). [doi](#)
25. H. Guo, L. Liu, Y. Wang, C. Hou, W. Li, M. Lu, K. Zou, and B. Peng, "Host dependence of spectroscopic properties of Dy³⁺-doped and Dy³⁺, Tm³⁺-codoped Ge-Ga-S-CdI₂ chalcogenide glasses," *Opt. Express* **17**, 15350 (2009). [doi](#)
26. M. Sun, A. Yang, H. Ren, Sisheng Qi, H. Lin, X. Feng, Zhiyong Yang, "Mid-infrared luminescence of dysprosium-doped gallium-antimony-sulfur-iodine chalcogenide glasses and fibers," *Journal of Non-Crystalline Solids* **560**, 120718 (2021) [doi](#)
27. T. Schweizer, D. W. Hewak, B. N. Samson, and D. N. Payne, "Spectroscopic data of the 1.8-, 2.9-, and 4.3-μm transitions in dysprosium-doped gallium lanthanum sulfide glass," *Opt. Lett.* **21**, 1594 (1996). [doi](#)
28. Y. Wan, J.C. Norman, Y. Tong, M.J. Kennedy, W. He, J. Selvidge, C. Shang, M. Dumont, A. Malik, H.K. Tsang, A.C. Gossard, J.E. Bowers, "Tunable quantum dot lasers grown directly on silicon," *Laser & Photonics Reviews* **14**, 2000037 (2020). [doi](#)
29. B. Cole, L.B. Shaw, P.C. Pureza, R. Mossadegh, J.S. Sanghera, I.D. Aggarwal, "Rare-earth doped selenide glasses and fibers for active applications in the near and mid-IR," *Journal of Non-Crystalline Solids* **256**, 253 (1999). [doi](#)
30. R.V. Kochanov, I.E. Gordon, L.S. Rothman, P. Wcislo, C. Hill, J.S. Wilzewski, "HITRAN Application Programming Interface (HAPI): A comprehensive approach to working with spectroscopic data," *J. Quant. Spectrosc. Radiat. Transfer* **177**, 15-30 (2016) [doi](#)